

# Mechanism of ferroelectric instabilities in non $d^0$ perovskites: $\text{LaCrO}_3$ versus $\text{CaMnO}_3$

Claude Ederer,\* Tim Harris, and Roman Kováčik  
*School of Physics, Trinity College Dublin, Dublin 2, Ireland*  
(Dated: August 5, 2021)

The incompatibility of partial  $d$  occupation on the perovskite  $B$ -site with the standard charge transfer mechanism for ferroelectricity has been a central paradigm in multiferroics research. Nevertheless, it was recently shown by density functional theory calculations that  $\text{CaMnO}_3$  exhibits a polar instability that even dominates over the octahedral tilting for slightly enlarged unit cell volume. Here, we present similar calculations for  $\text{LaCrO}_3$ , which has the same  $d^3$   $B$ -site electron configuration as  $\text{CaMnO}_3$ . We find that  $\text{LaCrO}_3$  exhibits a very similar, albeit much weaker, polar instability as  $\text{CaMnO}_3$ . In addition, while the Born effective charge (BEC) of the  $\text{Mn}^{4+}$  cation in  $\text{CaMnO}_3$  is highly anomalous, the BEC of  $\text{Cr}^{3+}$  in  $\text{LaCrO}_3$  is only slightly enhanced. By decomposing the BECs into contributions of individual Wannier functions we show that the ferroelectric instabilities in both systems can be understood in terms of charge transfer between TM  $d$  and  $O$   $p$  states, analogously to the standard  $d^0$  perovskite ferroelectrics.

## I. INTRODUCTION

The relative scarcity of multiferroic materials has often been explained by a chemical incompatibility between the factors that promote ferroelectricity compared to the factors that promote magnetic order.<sup>1,2</sup> Even though several mechanisms for ferroelectricity that are compatible with the simultaneous presence of magnetic cations have been identified recently (see e.g. Refs. 3–5), the most common mechanism for driving polar displacements in typical perovskite ferroelectrics seems to require a completely unoccupied  $d$  shell of the transition metal (TM) cations on the perovskite  $B$ -site. This statement is to some extent based on the observation, that essentially all known perovskite ferroelectrics (e.g.  $\text{BaTiO}_3$ ,  $\text{KNbO}_3$ ,  $\text{PbTiO}_3$ ,  $\text{Pb}(\text{Zr},\text{Ti})\text{O}_3$ , etc.) contain formal  $d^0$  TM cations on the  $B$ -site. On the other hand a partial filling of the electronic  $d$  states is required in order to create a magnetic moment,<sup>6</sup> and the resulting incompatibility has been a central paradigm in multiferroics research over the past few years.

The driving force behind the ferroelectric distortion in the  $d^0$  perovskites, such as e.g.  $\text{BaTiO}_3$  or  $\text{KNbO}_3$ , is related to hybridisation between the filled oxygen  $2p$  states and the empty  $d$  states of the TM cation.<sup>2,7,8</sup> A ferroelectric displacement reduces the distance between the TM cation and one or more of the surrounding oxygen anions, and thus strengthens the corresponding covalent bonds, while slightly weakening the bonds to the other surrounding oxygen anions where the corresponding bond distance is increased. This leads to an overall gain in covalent bond energy, which however is opposed by repulsive electro-static forces. The gain in hybridisation energy is maximal if the antibonding states with predominant TM  $d$  character are completely empty, and is zero if these antibonding states are completely filled.

Nevertheless, it has been shown recently that cubic perovskite  $\text{CaMnO}_3$  exhibits a similar ferroelectric instability which, even though it is rather weak at ambient conditions, can be significantly enhanced by applying negative pressure.<sup>9</sup> At the equilibrium lattice con-

stant the ferroelectric instability is suppressed by a much stronger antiferrodistortive instability, i.e. a collective tilting of the octahedral network, which leads to the observed  $Pbnm$ -distorted perovskite structure of  $\text{CaMnO}_3$ . This antiferrodistortive mode is rather independent of volume, so that the polar distortion becomes dominant for slightly increased lattice constant. Very similar behaviour has also been reported subsequently for  $\text{SrMnO}_3$  and  $\text{BaMnO}_3$ .<sup>10,11</sup> These calculations thus predict a new class of multiferroics, which could be synthesised for example as epitaxial thin films, where strain can stabilise the perovskite structure with enlarged lattice constant. However, the question of what is the driving force behind the ferroelectric instability in the corresponding systems, in particular whether it is related to the above-described charge transfer mechanism, has not been addressed in these previous studies.

Within a predominantly cubic crystal field, the  $d^3$  case of  $\text{CaMnO}_3$  can also be interpreted as  $e_g^0$  electron configuration, analogously to the  $d^0$  configuration found in most perovskite ferroelectrics. In this case the empty  $e_g$  states can in principle provide the increase in bond energy required for the ferroelectric instability, whereas the partial filling of the  $t_{2g}$  states can create a local magnetic moment. While the resulting gain in bond energy is probably smaller than for the case of a  $d^0$  TM cation, it is not obvious that this gain is necessarily always smaller than the opposing effect of the short range repulsion.<sup>2,4,11</sup> In fact, exactly this scenario has already been discussed in Ref. 2, and arguments were given that in addition to the usual repulsive forces, the Hund's rule coupling would further disfavour the ferroelectric instability in these cases.

Here we address the question of what is the driving force behind the ferroelectric instability in  $\text{CaMnO}_3$  and related systems. We clarify whether the ferroelectric distortion in these materials is driven by charge transfer between the TM cation and its surrounding oxygen anions, similar to the conventional  $d^0$  perovskite ferroelectrics. In order to investigate whether this effect is a peculiarity that is specific to the  $\text{Mn}^{4+}$  cation, or whether a simi-

lar polar instability can also be observed in other magnetic perovskites, we compare the case of  $\text{CaMnO}_3$  with  $\text{LaCrO}_3$ . Under equilibrium conditions  $\text{LaCrO}_3$  exhibits a  $Pbnm$ -distorted perovskite structure and G-type antiferromagnetic order,<sup>12</sup> similar to  $\text{CaMnO}_3$ . Furthermore, the  $\text{Cr}^{3+}$  cation on the perovskite  $B$  site has a  $d^3$  electron configuration that is iso-electronic to the  $\text{Mn}^{4+}$  cation in  $\text{CaMnO}_3$ .

We calculate phonon frequencies and eigenmodes at the  $\Gamma$ -point and at selected zone-boundary wave-vectors for  $\text{LaCrO}_3$  in the ideal perovskite structure at different volumes, and we then calculate and compare Born effective charges for  $\text{LaCrO}_3$ ,  $\text{CaMnO}_3$ , and the nonmagnetic ferroelectric  $\text{BaTiO}_3$ . Furthermore, we analyse the driving force for ferroelectric displacements in these three systems by decomposing the Born effective charges into contributions of individual Wannier functions.

## II. COMPUTATIONAL DETAILS

All results presented in this report are obtained using the Quantum ESPRESSO package, employing a plane wave basis set and ultrasoft pseudopotentials.<sup>13,14</sup> A plane-wave kinetic energy cutoff of 35 Ry (420 Ry) is used for the expansion of the wave-functions (charge density). The  $3s$  and  $3p$  semi-core states of Cr, Mn, and Ca, as well as the  $5s$  and  $5p$  states of La, are included in the valence. Different k-point meshes are used to calculate the different quantities presented in this work, with convergence verified in all cases. Calculations are performed using both the Generalised Gradient Approximation (GGA) and the GGA+ $U$  approach with  $U_{\text{eff}} = 4$  eV applied to the TM  $d$  states.<sup>15,16</sup>

## III. RESULTS

### A. Phonon calculations

Similar to Ref. 9, we first identify potential phonon instabilities in cubic  $\text{LaCrO}_3$  by calculating eigenfrequencies of all zone-centre and various selected zone-boundary modes at different lattice constants. We investigate variations of  $\pm 3\%$  around an average lattice constant  $a = 3.89$  Å, which corresponds to the same volume per formula unit as in the experimentally observed  $Pbnm$  structure of  $\text{LaCrO}_3$ .<sup>12</sup> The relevant zone-boundary modes are selected by decomposing the structural distortion between ideal  $Pm\bar{3}m$  symmetry and the experimental  $Pbnm$  structure into symmetry adapted modes, and then identifying the main components in this decomposition. The ISODISPLACE utility is used for the mode decomposition.<sup>17</sup> The dynamical matrix is obtained from the calculated forces created by small finite displacements of the individual ions.

We find two strongly unstable antiferrodistortive zone-boundary modes ( $R_5^-$  and  $M_2^+$ ), which are responsible for

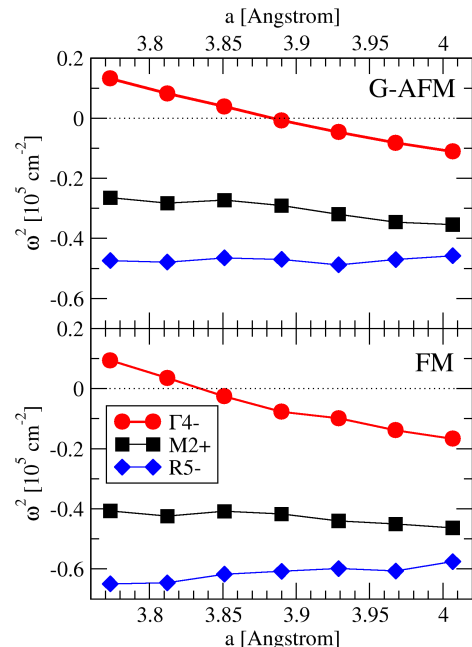


FIG. 1: Calculated eigenvalues  $\omega^2$  of the dynamical matrix of cubic  $\text{LaCrO}_3$  for selected modes as function of cubic lattice parameter  $a$  using  $U_{\text{eff}} = 4$  eV. The upper panel corresponds to G-type antiferromagnetic order (G-AFM), the lower panel to the ferromagnetic case (FM). Negative  $\omega^2$  indicates a structural instability.

the experimentally observed  $Pbnm$  ground state structure, and a soft polar ( $\Gamma_4^-$ ) mode, which is unstable for larger lattice constants.<sup>18</sup> The corresponding results are presented in Fig. 1 for both the ground state G-type antiferromagnetic order and the ferromagnetic case. Similar to  $\text{CaMnO}_3$ , the antiferrodistortive modes are rather insensitive to volume, whereas the polar mode is strongly volume-dependent. It can also be seen that ferromagnetic order leads to a further destabilisation of all modes. This is a result of the fact that the antiferromagnetic superexchange interaction is strongest for an ideal  $180^\circ$  TM-O-TM bond angle. In the magnetically unfavourable ferromagnetic case the energy of the system can therefore be lowered by distorting the bond angle away from  $180^\circ$ .

It is clear from these results that qualitatively  $\text{LaCrO}_3$  behaves very similar to  $\text{CaMnO}_3$ . However, on a quantitative level, the polar instability is significantly weaker in  $\text{LaCrO}_3$  than in  $\text{CaMnO}_3$  ( $\omega^2 = -0.11 \cdot 10^5 \text{ cm}^{-2}$  for +3% expansion in lattice constant, compared to  $\omega^2 = -0.36 \cdot 10^5 \text{ cm}^{-2}$  for +2% expansion in  $\text{CaMnO}_3$ ). Even at rather large volume, the polar instability in  $\text{LaCrO}_3$  never dominates over the antiferrodistortive modes.<sup>19</sup>

### B. Born effective charges

To further analyse the differences and similarities between  $\text{LaCrO}_3$  and  $\text{CaMnO}_3$ , we calculate the Born effective charges (BECs) of the  $B$ -site cations in both systems.

TABLE I: Born effective charges  $Z_{zz}^*$  of the TM cations in the three systems under consideration, calculated using the Berry phase approach, and compared to previously reported values and to the corresponding formal charges.

	BaTiO <sub>3</sub>	LaCrO <sub>3</sub>	CaMnO <sub>3</sub>
formal charge	4	3	4
$U_{\text{eff}} = 0$ eV	7.31	3.62	7.61
$U_{\text{eff}} = 4$ eV	—	3.58	7.66
previous work ( $U_{\text{eff}} = 0$ eV)	7.25 <sup>21</sup>	3.76 <sup>22</sup>	8.16 <sup>9</sup>
	6.89 <sup>8</sup>		6.99 <sup>8</sup>

The BEC tensor  $Z_{i,\alpha\beta}^*$  describes the change in polarisation component  $P_\alpha$  resulting from a displacement of ion  $i$  along Cartesian direction  $\beta$ .<sup>20,21</sup>

$$Z_{i,\alpha\beta}^* = \frac{\Omega}{|e|} \frac{\partial P_\alpha}{\partial r_{i,\beta}} \quad . \quad (1)$$

Here,  $\Omega$  is the unit cell volume and  $e$  is the electronic charge. Anomalously enhanced BECs (compared to the formal charge value) indicate that the corresponding displacements lead to strong changes in hybridisation with the surrounding ions, and are generally interpreted as “smoking gun” for the charge transfer mechanism towards ferroelectricity described in Sec. I.<sup>20,21</sup>

We calculate BECs from the change in polarisation corresponding to small finite displacements of the TM cations along the cubic axes. The electric polarisation is calculated in two different ways: i) by using the Berry phase approach,<sup>23,24</sup> and ii) by constructing maximally localised Wannier functions (MLWFs) and monitoring changes in the centres of gravity of the individual Wannier orbitals.<sup>25,26</sup> The BECs obtained using the Berry-phase approach are listed in Table I. In addition to the BECs of the Mn and Cr cations in CaMnO<sub>3</sub> and LaCrO<sub>3</sub>, respectively, the BEC for the Ti<sup>4+</sup> cation in the prototypical ferroelectric BaTiO<sub>3</sub> is also calculated.<sup>27</sup>

It can be seen from Table I that the effect of  $U_{\text{eff}}$  on the BECs is small and that all calculated values agree well with previously reported data. Furthermore, in agreement with Ref. 9, the BEC of Mn<sup>4+</sup> in CaMnO<sub>3</sub> is very strongly enhanced compared to the formal charge of +4. The anomalous part of the BEC amounts to about 90 % of the formal charge (or  $\sim 3.65$  electrons), very similar to the enhancement observed for the Ti<sup>4+</sup> cation in BaTiO<sub>3</sub>. On the other hand the BEC of Cr<sup>3+</sup> in LaCrO<sub>3</sub> is only increased by a factor of 1.2 (or 0.6 electrons) compared to the formal charge of +3. Thus, the differences in the BECs between LaCrO<sub>3</sub> and CaMnO<sub>3</sub> seem consistent with the significantly weaker polar instability of LaCrO<sub>3</sub> compared to CaMnO<sub>3</sub>. However, we also point out that there is no straightforward relationship between the magnitude of the BECs and the tendency of a certain material towards ferroelectricity (otherwise CaMnO<sub>3</sub> should be just as ferroelectric as BaTiO<sub>3</sub>).

TABLE II: Decomposition of Born effective charges  $Z_{zz}^*$  of the  $B$  site cation in contributions of individual Wannier centres. Contributions of oxygen-centred MLWFs are averaged over both spin-projections, whereas TM  $t_{2g}$  contributions correspond to the local majority spin-projection. All values are calculated for  $U_{\text{eff}} = 0$ .

		BaTiO <sub>3</sub>	LaCrO <sub>3</sub>	CaMnO <sub>3</sub>
Mn/Cr	$d_{xy}(\uparrow)$	—	-1.081	-1.019
Mn/Cr	$d_{xz}/d_{yz}(\uparrow)$	—	-1.111	-1.002
O( $z$ )	$p_x/p_y$	0.853	0.239	0.516
O( $z$ )	$p_z$	0.330	0.347	1.067
O( $z$ )	$s$	0.267	0.212	0.331
O( $y$ )	$p_x$	-0.0812	-0.059	-0.088
O( $y$ )	$p_y$	-0.141	-0.217	-0.300
O( $y$ )	$p_z$	-0.092	0.023	0.165
O( $y$ )	$s$	-0.072	-0.129	-0.124
total valence		3.065	-2.760	0.451
semi-core		-7.716	-7.628	-7.877
ionic core		12.000	14.000	15.000
total BEC		7.349	3.612	7.573
formal		4	3	4

### C. Wannier decomposition of BECs

To further analyse the origin of the enhanced BECs in the three investigated systems, we decompose the electric polarisation calculated via MLWFs into contributions of the individual Wannier orbitals  $|w_n\rangle$ :<sup>26</sup>

$$P = P_{\text{ionic core}} - \frac{|e|}{\Omega} \sum_n \langle w_n | r | w_n \rangle \quad . \quad (2)$$

This translates into a corresponding decomposition of the BECs:

$$Z^* = Z_{\text{ionic core}} + \sum_n Z_n^* \quad , \quad (3)$$

with:

$$Z_n^* = - \frac{\Delta r_n}{\Delta r_{\text{ion}}} \quad (4)$$

Here,  $\Delta r_n = \langle w_n(\Delta r_{\text{ion}}) | r | w_n(\Delta r_{\text{ion}}) \rangle - \langle w_n(0) | r | w_n(0) \rangle$  is the displacement of the Wannier centre  $n$  resulting from the ionic displacement  $\Delta r_{\text{ion}}$ .

For each of the three systems under consideration, the occupied valence and semi-core states form energetically isolated groups of bands with a specific dominant atomic and orbital character: TM semi-core  $3s$  and  $3p$ ,  $A$ -site cation semi-core  $s$  and  $p$ , and oxygen  $2s$  and  $2p$ . In the case of LaCrO<sub>3</sub> and CaMnO<sub>3</sub>, the oxygen  $2p$  bands are inter-mixed with the local majority spin TM  $t_{2g}$  states. We construct separate MLWFs for each isolated set of occupied bands using the Wannier90 code.<sup>29</sup> The resulting MLWFs exhibit a clear atomic and angular momentum

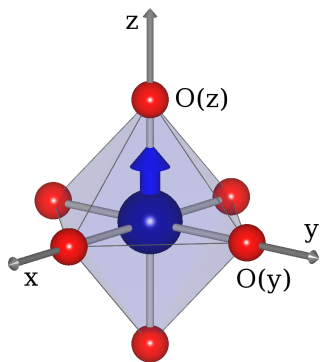


FIG. 2: Geometry for the calculation of BECs listed in Table II.  $O(y)$  and  $O(z)$  are the oxygen anions situated adjacent to the displaced TM cation along the  $y$  and  $z$  directions, respectively. The thick arrow indicates the displacement direction ( $z$  direction). Picture generated using VESTA.<sup>28</sup>

( $lm$ ) character, albeit with a certain amount of admixture of other atomic orbitals on the surrounding ions due to hybridisation (see Fig. 3 for some examples). We use this atomic and orbital character to label each MLWF. The individual contributions to the TM cation BECs of all individual valence MLWFs as well as the sum over all semi-core contributions are listed in Table II.  $O(z)$  and  $O(y)$  denote the two symmetry inequivalent oxygen anions situated along and perpendicular to the displacement direction of the TM cation (see Fig. 2). It can be seen that the values for the total BECs calculated via MLWFs which are listed in Table II are in good agreement with the values calculated via the Berry-phase approach listed in Table I. The individual contributions to the BECs for  $\text{BaTiO}_3$  are also in good agreement with results of a similar decomposition presented in Ref. 30.

Within a completely ionic picture, i.e. without inter-site hybridisation, the contributions to the BECs from the occupied TM  $t_{2g}$  orbitals in  $\text{LaCrO}_3/\text{CaMnO}_3$  would be exactly equal to  $-1$ , whereas the contributions from all oxygen orbitals would be identically zero. In addition, with the core/valence separation used in our pseudopotentials, the total contribution of all semi-core states would be exactly equal to  $-8$  for all three systems. The  $t_{2g}$  contributions to the BECs in both  $\text{LaCrO}_3$  and  $\text{CaMnO}_3$  are indeed very close to the nominal value of  $-1$ , and the semi-core contributions to  $Z^*$  are also close to  $-8$ , deviating only by about 0.1-0.4 electrons from this value. In contrast, strong anomalous contributions are found for the oxygen  $s$  and  $p$  orbitals, with the largest contributions resulting from the  $p$  orbitals corresponding to the oxygen anions  $O(z)$  situated above and below the  $B$ -site cation along the displacement direction ( $z$ -direction, see Fig. 2).

The large positive contributions of these orbitals indicate that the centres of the corresponding MLWFs shift towards the TM cation that is moved closer to the oxygen. This represents a net electron flow from the oxygen

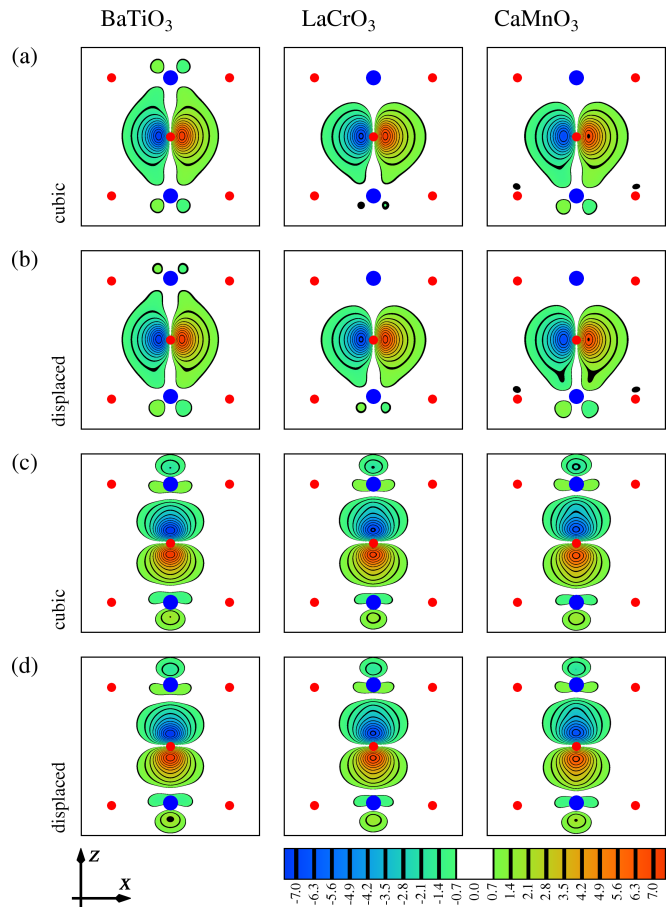


FIG. 3: (Color online) Maximally localised Wannier functions corresponding to  $\pi$ -oriented  $p_x$  orbitals ((a), (b)) and  $\sigma$ -oriented  $p_z$  orbitals ((c), (d)) centred on  $O(z)$  for  $\text{BaTiO}_3$  (left column),  $\text{LaCrO}_3$  (middle column) and  $\text{CaMnO}_3$  (right column). (a) and (c) correspond to the cubic structures, whereas in (b) and (d) the TM cations were displaced along  $+z$  by 1% of the cubic lattice constants. Shown are cuts through the  $x$ - $z$  plane. The positions of the oxygen anions/TM cations are indicated by the filled small/large (red/blue) circles.

anion towards the TM cation. Fig. 3 depicts the changes in the  $O(z)$   $p$  MLWFs for a displacement of the TM cation along  $+z$  by 1% of the cubic perovskite lattice constant. We point out that this displacement is much larger than the one used for the calculation of the BECs (which was only  $\sim 0.2\%$ ). A larger displacement was used in Fig. 3 to make the changes in the MLWFs more visible. It can be seen that the displacement of the TM cation towards the oxygen anion increases the amplitude of the corresponding atomic  $d$  character in the  $O(z)$   $p$  MLWFs compared to the cubic case. This change in hybridisation shifts the centre of the Wannier function towards the closer TM cation, leading to the anomalous contribution to the BECs.

In  $\text{BaTiO}_3$ , where the Ti  $d$  states are empty and therefore do not contribute to the polarisation, the anomalous contribution to the BECs listed in Table II are strongest for the  $\pi$ -type ( $p_x/p_y$ ) orbitals, i.e. for the  $p$  orbitals

that are oriented perpendicular to the Ti-O bond and hybridise with the empty  $t_{2g}$  states on the Ti cation. The contribution of the  $\sigma$ -type ( $p_z$ ) orbital, which hybridises with the Ti  $e_g$  states, is more than a factor of two smaller.

If we compare this to the case of  $\text{LaCrO}_3$ , where the majority spin  $t_{2g}$  states are filled, the relative contributions of the two types of  $p$  states change significantly. The contribution of the  $p_z$  orbital is very similar to the case of  $\text{BaTiO}_3$ , but the contributions of the  $p_x$  and  $p_y$  orbitals are strongly reduced and are now smaller than the  $p_z$  contribution.

This effect is related to a strong reduction of the  $d$ -like “tails” in the  $O(z)$   $p_x$  and  $p_y$  MLWFs in  $\text{LaCrO}_3$  compared to  $\text{BaTiO}_3$ , which can be seen from Fig. 3a and Fig. 3b. In  $\text{BaTiO}_3$ , these tails represent the TM  $d$  character contained in the nominal oxygen  $p$  bands, which, as discussed in the introductory paragraphs, are *bonding* states that result from hybridisation between atomic TM  $d$  and oxygen  $p$  orbitals. Once the corresponding *antibonding* states (or parts thereof) become occupied, the different orbital contributions can be separated into different MLWFs with appropriate orbital character.

More specifically, we note that the MLWFs shown in Fig. 3 correspond to the global “spin-up” projection. For  $\text{BaTiO}_3$  the two spin-projections are of course identical, whereas for the magnetic systems the “spin-up” and “spin-down” MLWFs centred at  $O(z)$  are related to each other by space inversion. For the specific cases shown in Fig. 3 the local magnetic moment of the Cr/Mn cation located at  $+\frac{a}{2}\hat{z}$  relative to the central oxygen anion is parallel to the global spin-up direction, whereas the local magnetic moment of the Cr/Mn cation at  $-\frac{a}{2}\hat{z}$  is parallel to the global spin-down direction. It can be seen that the  $t_{2g}$ -tails of the  $p_x$  MLWFs at  $+\frac{a}{2}\hat{z}$  have completely vanished. This is due to the effect described above, i.e. the corresponding orbital character has been transferred to the  $t_{2g}(\uparrow)$  MLWFs. In addition, the  $t_{2g}$ -tail at  $-\frac{a}{2}\hat{z}$  is also significantly reduced, because the global spin-up direction at this TM site correspond to the local minority spin character. The corresponding  $t_{2g}$  states are therefore higher in energy, which reduces the amount of  $p$ - $t_{2g}$  hybridisation at this site. As a result, the  $p_x/p_y$  MLWFs in  $\text{LaCrO}_3$  resemble more closely the corresponding atomic orbitals compared to the  $p_x/p_y$  MLWFs in  $\text{BaTiO}_3$ , and the contributions to the BECs become less anomalous.

The same hierarchy between the  $p_x/p_y$  and  $p_z$  contributions as in  $\text{LaCrO}_3$  can be observed for  $\text{CaMnO}_3$ , but the overall magnitude of both contributions is strongly enhanced in the latter. The contribution of the  $O(z)$   $p_z$  MLWF in  $\text{CaMnO}_3$  is even three times larger than the corresponding contribution in  $\text{BaTiO}_3$ .

#### D. Densities of states

The origin of the strong enhancement of the individual contributions to the BECs in  $\text{CaMnO}_3$  can be ra-

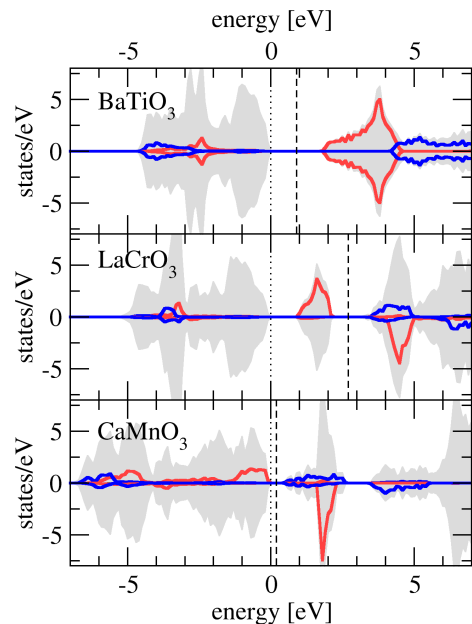


FIG. 4: (Color online) Spin-resolved total and projected DOS for cubic  $\text{BaTiO}_3$  (top),  $\text{LaCrO}_3$  (middle), and  $\text{CaMnO}_3$  (bottom), calculated within GGA. The shaded curves represent the total DOS, the bright/dark (red/blue) lines represent the  $t_{2g}/e_g$  projected DOS of the  $B$ -site cations. Different spin projections are shown with different sign. For better comparison, the DOS are aligned to the top of the oxygen  $p$  bands. Mid-gap (Fermi) levels are indicated by dashed vertical lines.

tionalised by looking at the differences in the electronic structure of the three materials. The total and projected densities of states (DOS) for  $\text{BaTiO}_3$  (nonmagnetic),  $\text{LaCrO}_3$ , and  $\text{CaMnO}_3$  (both G-type AFM) are shown in Fig. 4. It can be seen that in  $\text{BaTiO}_3$  and  $\text{LaCrO}_3$  the TM  $d$  bands are situated well above the oxygen  $p$  bands. In particular the bottom of the TM  $e_g$  states is about 3.5-4 eV above the top of the predominantly oxygen  $p$  bands in both systems. On the other hand in  $\text{CaMnO}_3$  the corresponding energy separation is much smaller, with the bottom of the Mn  $e_g$  states only about 0.5 eV above the oxygen  $p$  bands. This small energy separation leads to very strong hybridisation between oxygen  $p$  and TM  $d$  levels in  $\text{CaMnO}_3$ . The much stronger hybridisation in  $\text{CaMnO}_3$  compared to both  $\text{LaCrO}_3$  and  $\text{BaTiO}_3$  will thus enhance all resulting effects, including the anomalous contributions to the BECs. The strong hybridisation in  $\text{CaMnO}_3$  therefore compensates the reduced  $p_x/p_y$  contribution relative to  $p_z$ , leading to the large total BEC (of the same magnitude as in  $\text{BaTiO}_3$ ) and the rather strong polar instability compared to  $\text{LaCrO}_3$ .

As a final technical note, we point out that the weak effect of  $U_{\text{eff}}$  on the BECs in  $\text{CaMnO}_3$  and  $\text{LaCrO}_3$  is a result of the specific projection on (non-orthogonal) atomic orbitals used for the LSDA+ $U$  implementation within Quantum ESPRESSO. For both  $\text{LaCrO}_3$  and  $\text{CaMnO}_3$  the resulting orbital occupation matrix element corre-

sponding to the majority spin  $e_g$  states is approximately equal to 0.5. Since the LSDA+ $U$  potential shift of the TM  $d$  states is given by  $\Delta V_m^\sigma = \frac{U_{\text{eff}}}{2}(\frac{1}{2} - n_m^\sigma)$ ,<sup>16</sup> the energy separation between the  $e_g$  states and the oxygen  $p$  bands is thus not affected by the value of  $U_{\text{eff}}$  for  $n_{e_g}^\uparrow \approx 0.5$ . According to the preceding discussion it is essentially this energy difference that determines the magnitude of the anomalous contribution to the TM BECs in LaCrO<sub>3</sub> and CaMnO<sub>3</sub>, which are therefore rather independent of  $U_{\text{eff}}$ .

#### IV. SUMMARY AND CONCLUSIONS

In summary, we have shown that LaCrO<sub>3</sub> exhibits a strongly volume-dependent polar instability very similar to CaMnO<sub>3</sub>. However the polar instability is significantly weaker in LaCrO<sub>3</sub> than in CaMnO<sub>3</sub>. This is consistent with the much less anomalous BEC of the Cr<sup>3+</sup> cation in LaCrO<sub>3</sub> compared to the strongly enhanced BEC of Mn<sup>4+</sup> in CaMnO<sub>3</sub>. By decomposing the BECs in contributions of individual Wannier functions, we could show that in both cases the largest anomalous contributions stem from  $\sigma$ -oriented O  $p$  states of the oxygen anions

adjacent to the TM cation along the displacement direction, whereas the corresponding  $\pi$  contributions are reduced compared to the  $d^0$  ferroelectric BaTiO<sub>3</sub>. This reduction of the  $\pi$ -type contributions to the BECs relative to the  $\sigma$ -type contribution is due to the occupation of the majority spin  $t_{2g}$  states in LaCrO<sub>3</sub> and CaMnO<sub>3</sub>. The strong overall enhancement of the anomalous charges in CaMnO<sub>3</sub> can be explained by the near degeneracy of O  $p$  and TM  $d$  states in CaMnO<sub>3</sub>, which leads to very strong hybridisation and thus enhances all related effects. The polar instabilities in both magnetic perovskites can therefore be understood in terms of charge transfer between TM  $d$  and O  $p$  states, analogously to the standard  $d^0$  perovskite ferroelectrics.

#### Acknowledgments

This work was supported by Science Foundation Ireland under grant numbers SFI-07/YI2/I1051 (PIYRA) and SFI-UR-I1531 (SURE UREKA site), and made use of computational facilities provided by the Trinity Centre for High Performance Computing.

- 
- \* Electronic address: ederer@tcd.ie
- <sup>1</sup> N. A. Hill, J. Phys. Chem. B **104**, 6694 (2000).
  - <sup>2</sup> D. I. Khomskii, J. Magn. Magn. Mater. **306**, 1 (2006).
  - <sup>3</sup> S.-W. Cheong and M. Mostovoy, Nature Materials **6**, 13 (2007).
  - <sup>4</sup> D. Khomskii, Physics **2**, 20 (2009).
  - <sup>5</sup> S. Picozzi and C. Ederer, J. Phys.: Condens. Matter **21**, 303201 (2009).
  - <sup>6</sup> In the present discussion we do not consider  $f$ -electron magnetism.
  - <sup>7</sup> R. E. Cohen, Nature **358**, 136 (1992).
  - <sup>8</sup> A. Filippetti and N. A. Hill, Phys. Rev. B **65**, 195120 (2002).
  - <sup>9</sup> S. Bhattacherjee, E. Bousquet, and P. Ghosez, Phys. Rev. Lett. **102**, 117602 (2009).
  - <sup>10</sup> J. H. Lee and K. M. Rabe, Phys. Rev. Lett. **104**, 207204 (2010).
  - <sup>11</sup> J. M. Rondinelli, A. S. Eidelson, and N. A. Spaldin, Phys. Rev. B **79**, 205119 (2009).
  - <sup>12</sup> G. Li, X. Kuang, S. Tian, F. Liao, X. Jing, Y. Uesu, and K. Kohn, J. Solid State Chem. **165**, 381 (2002).
  - <sup>13</sup> P. Gianozzi, S. Baroni, N. Bonini, M. Calandra, R. Car, C. Cavazzoni, D. Ceresoli, G. L. Chiarotti, M. Cococcioni, I. Dabo, et al., J. Phys.: Condens. Matter **21**, 395502 (2009).
  - <sup>14</sup> D. Vanderbilt, Phys. Rev. B **41**, 7892 (1990).
  - <sup>15</sup> J. P. Perdew, K. Burke, and M. Ernzerhof, Phys. Rev. Lett. **77**, 3865 (1996).
  - <sup>16</sup> S. L. Dudarev, G. A. Botton, S. Y. Savrasov, C. J. Humphreys, and A. P. Sutton, Phys. Rev. B **57**, 1505 (1998).
  - <sup>17</sup> B. J. Campbell, H. T. Stokes, D. E. Tanner, and D. M. Hatch, J. Appl. Crystallogr. **39**, 607 (2006).
  - <sup>18</sup> These symmetry labels correspond to a definition of the perovskite structure with the  $A$ -site at the origin.
  - <sup>19</sup> We have verified that the calculated phonon eigenvalues do not depend strongly on the specific value of  $U_{\text{eff}}$  used in the calculation.
  - <sup>20</sup> W. Zhong, R. D. King-Smith, and D. Vanderbilt, Phys. Rev. Lett. **72**, 3618 (1994).
  - <sup>21</sup> P. Ghosez, J. P. Michenaud, and X. Gonze, Phys. Rev. B **58**, 6224 (1998).
  - <sup>22</sup> N. Ray and U. V. Waghmare, Phys. Rev. B **77**, 134112 (2008).
  - <sup>23</sup> R. D. King-Smith and D. Vanderbilt, Phys. Rev. B **47**, (1993).
  - <sup>24</sup> R. Resta, Rev. Mod. Phys. **66**, 899 (1994).
  - <sup>25</sup> N. Marzari and D. Vanderbilt, Phys. Rev. B **56**, 12847 (1997).
  - <sup>26</sup> D. Vanderbilt and R. D. King-Smith, Phys. Rev. B **48**, 4442 (1993).
  - <sup>27</sup> The BEC of Ti in BaTiO<sub>3</sub> was calculated within GGA for a cubic perovskite structure with lattice constant  $a = 3.93 \text{ \AA}$ , which corresponds to the theoretical lattice constant reported in Ref. 8. For CaMnO<sub>3</sub>, the same lattice constant as in Ref. 9 ( $a = 3.74 \text{ \AA}$ ) was used to calculate the BEC.
  - <sup>28</sup> K. Momma and F. Izumi, J. Appl. Crystallogr. **41**, 653 (2008).
  - <sup>29</sup> A. A. Mostofi, J. R. Yates, Y.-S. Lee, I. Souza, D. Vanderbilt, and N. Marzari, Comp. Phys. Comm. **178**, 685 (2008).
  - <sup>30</sup> N. Marzari and D. Vanderbilt, in *First principles calculations for ferroelectrics: Fifth Williamsburg workshop*, edited by R. E. Cohen (AIP, Woodbury, New York, 1998).